Scanning-less Optical Near-Field Characterization for Structured Light Fields Based on Nonlinear Effect

Zhenli Li(李振锂)†, Rongyi Lin(林荣裔)†, Min Lin (林旻)*, Luping Du (杜路平) and Xiaocong Yuan(袁小聪)

Nanophotonics Research Center, Institute of Microscale Optoelectronics & State Key Laboratory of Radio Frequency Heterogeneous Integration, Shenzhen University, Shenzhen 518060, China

†These authors contributed equally to this work.

*Corresponding author: min.lin.s12@gmail.com

Conventional methods for near-field characterization typically relied on the nanoprobe to point-scan the field, rendering the measurements vulnerable to external environmental influences. Here, we study on the direct far-field imaging of the near-field polarizations based on the four-wave mixing effect. We construct a simulation model to realize the instantaneous extraction of the near-field distributions of a wide range of structured light fields, such as cylindrical vector vortex beams, plasmonic Weber beams, and topological spin textures including photonic skyrmions and merons. This method is valuable for the studies on manipulation of structured light fields and light-matter interaction at micro/nano scales.

***Keywords**: Scanning-less* optical near-field detection; Near-to-far-field transform; Nonlinear effect; Structured light fields; Topological quasi-particles

1. Introduction

The technique of characterizing the optical field in the near-field region, as exemplified by near-field scanning optical microscopy (NSOM)[1], has been extensively employed for investigating surface plasmon polaritons (SPPs)[2,3], surface wave conduction of inorganic materials[4], photoionization of two-dimensional materials[5,6], near-field photocurrents[7,8], and semiconductor carrier concentration[9,10]. In nanophotonics, this technique provides a means to observe and study the physical properties of light fields at micro/nano scales, which exhibit distinct characteristics compared to their macroscopic counterparts. Moreover, it offers valuable insights into unique phenomena that emerge from interactions between light and micro/nanostructures. Consequently, this technique plays a pivotal role in investigating novel physical phenomena and advancing innovative applications.

However, the conventional imaging process of NSOM requires point-by-point scanning of the nanoprobes, which prolongs the imaging time and increases the system's complexity, rendering the measurements vulnerable to external environmental influences, such as platform vibration and temperature fluctuations during the scanning process[11]. In addition, the intrusion of the nanoprobe into the evanescent field can disturb the field to some extent, affecting the accuracy of measurements[12]. Moreover, the nanoprobe may collide with the

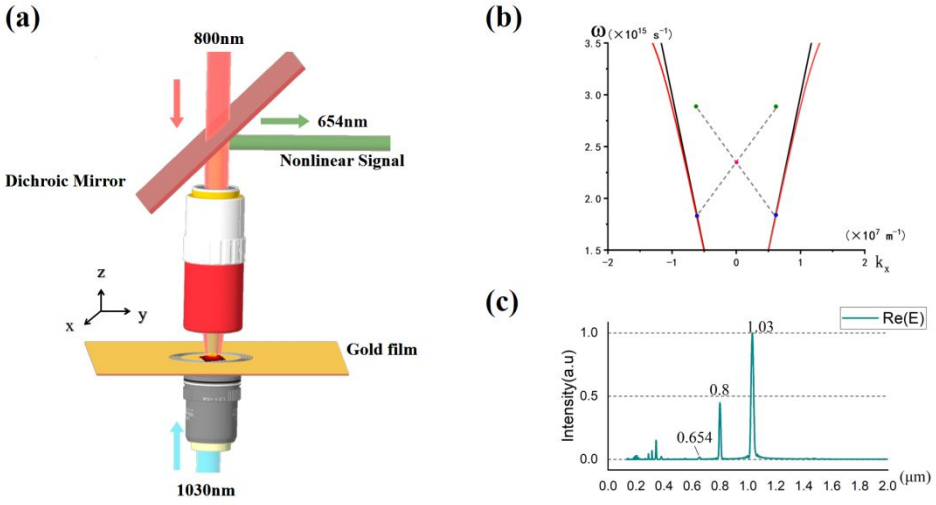

Fig. 1 (a) Schematic diagram of the nonlinear process. (b) Dispersion curve of SPP on gold film surface (red line) and dispersion curve of photons in vacuum (black line), pump photon (pink), SPP (blue) and nonlinear photon （green） are connected by blue dashed lines, which represent the partially degenerate four-wave mixing interaction. (c) Spectrum detected at 5nm above the gold film in simulation when the four wave-mixing happens.

sample during the scanning process when the measured area is not sufficiently flat, leading to potential damage of the sample and reduced lifespan of the nanoprobe. As a result, such methods are unsuitable for samples with time-varying light fields and complicated nanostructure.

Recently, a method for converting near-field optical information to far-field radiation based on the nonlinear effect has been proposed[13,14]. This mechanism is different from the traditional NSOM, which needs to introduce nanoprobes in the near-field optical field to realize the scattering of the near-field information to the far-field radiation. Instead, the near-field information can be encoded into the nonlinear signal propagating in the far-field, and the direct detection of near-field optical field information in the far-field can be realized. Moreover, compared to the NSOM's inability to differentiate different polarizations, this nonlinear near-field characterization method can extract different in-plane near-field polarizations to reconstruct the 3D electric field vectors and photonic spin vectors.

In the realm of light field manipulation, a wide range of complicated structured light field has been discovered continuously. Especially, recent discoveries of photonic topological quasi-particles, such as skyrmions[15,16], merons[17,18], and hopfions[19,20], have garnered significant interest. Due to the stabilities protected by topology and deep-subwavelength features, the photonic-skyrmion-related topological spin textures have demonstrated potential applications in optical information storage[21], picometre metrology[22], and magnetic domain detection[23]. The investigation and manipulation of the complicated structured light field exemplified by photonic skyrmion necessitate the development of near-field characterization technique capable of measuring time-varying light fields and different polarizations.

In this work, we investigate the direct far-field imaging of the near-field polarization utilizing the four-wave mixing effect, which can be applied in the scanning-less near-field characterization of the structured light fields. We construct a simulation model through analysis of nonlinear coefficients, and the transformation from the near-field polarization distributions to the far-field nonlinear signals has been realized for a wide range of complicated structured light fields, such as cylindrical vector vortex beams, plasmonic Weber beams (PWB), and topological spin textures including photonic skyrmions and merons. It provides a simulation tool to guide further scanning-less near-field characterization experiments in the future, which is of great value to the dynamic observations and manipulations of the structured light fields, as well as the nonradiative optical modes such as bound states in the continuum (BIC)[24,25]. Moreover, this constructed simulation model extends beyond the four-wave mixing nonlinear process, and can be utilized for the guidance of a wide range nonlinear interactions involving multiple sources such as the sum frequency and difference frequency generations and the related investigations.

2. Method

The scanning-less imaging capability of nonlinear optical near-field microscopy (NNOM) stems from a nonlinear process known as partially degenerate four-wave mixing (FWM). In the FWM process, the nonlinear signal photons are generated from the interaction between two pump light photons and the near-field photons, exemplified by the SPPs at the metal-dielectric interface. This process transforms the spatial information stored in a near-field wave pattern into nonlinear signals propagating in free space, which can then be directly captured by a CCD. An illustration of this nonlinear interaction is shown in Fig. 1(a). The pump light (800nm) is approximately vertically incident on the gold film, which is focused by a long working-distance objective lens to increase power density. This area is exactly the location of the SPP field which is generated via the process that the excitation light (1030nm) is focused with an objective lens and then illuminates the gratings. When the wave vector matching condition is satisfied, the nonlinear polarization field radiates to the far-field and is collected by the same long-working-distance objective and separated by the dichroic mirror from the background. At last, the nonlinear signal could be collected with a CCD.

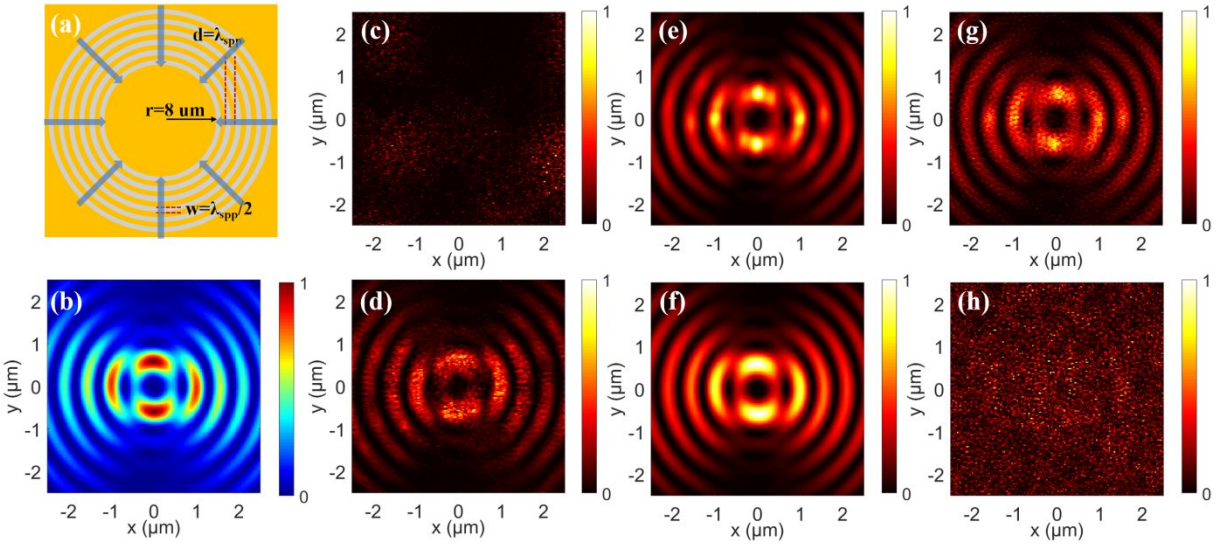

Fig. 2 (a) Schematics of grating structure used to excite SPP. The arrow (blue) represents the polarization direction of the excitation light, which is radially polarized. (b) The E_x component of the SPP field generated by third-order vortex radially polarized light incident on the grating. (c–h) The nonlinear signal with the x-polarization pump light when the coefficient is set as (c) 1.2×10^{-4} (m/v)², (d) 10^{-4} (m/v)², (e) 10^{-6} (m/v)², (f) 10^{-7} (m/v)², (g) 10^{-8} (m/v)², and (h) 10^{-9} (m/v)², respectively

In the nonlinear near-field characterization process involving SPPs, the photon momentum conservation and transverse wave vector matching conditions in the FWM process can be described as follows[26]:

$$\omega_{nl} = 2\omega_{pump} - \omega_{spp} \tag{1}$$

$$k_{nl,\mathrm{P}} = 2k_{pump,\mathrm{P}} - k_{spp,\mathrm{P}} \tag{2}$$

where ω_{nl}、 ω_{pump} and ω_{spp} refer to the frequency of the nonlinear signal light, pump light, and SPP, $k_{nl,\mathrm{P}}$、 $k_{pump,\mathrm{P}}$ and $k_{spp,\mathrm{P}}$ refer to the components of the nonlinear signal light, pump light, and SPP vector in the direction of the wave vector parallel to the surface of the metal. For pump light focused with a long-working distance objective lens vertically incident onto the metal surface, the transverse wave vector $k_{pump,\mathrm{P}} \approx 0$, thus $k_{\mathrm{nl,P}} = -k_{\mathrm{spp,P}}$. The in-plane information of the near-field is encoded into the generated new frequency nonlinear signal field. In this process, the nonlinear photon is inside the light cone compared to the corresponding near-field photon which is outside the light cone, as shown in Fig. 1(b). When the in-plane wave vector component of the nonlinear polarized field is smaller than its wave vector component in free space at a certain frequency, it will radiate to the far field which means the information of SPP can be measured via the signal of nonlinear light field, thereby enabling the retrieval of the near-field local information from the transformed light wavefield.

According to the symmetry governed nonlinear selection rule, the third-order nonlinear effect exist in materials exhibiting $C2$ symmetry, a characteristic that is frequently observed in various materials. Therefore, this near-field mapping process based on third-order nonlinear effects can be applied to a wide range of materials. In this work, gold is utilized for excitation of nonlinear signals, characterized by a face-centered cubic crystal structure that conforms to $C2$ symmetry.

Moreover, the polarization component of the near-field mapped by the nonlinear signal can be selected by the polarization of the pump beam, which satisfies the relation[27]:

$$E_{nl,x} \overset{E_{pump,x}}{\propto} E_{spp.x} \tag{3}$$

$$E_{nl,\sigma_\pm} \overset{E_{pump,\sigma_\pm}}{\propto} E_{spp,\sigma_\pm} \tag{4}$$

where $\sigma_\pm = \frac{\sqrt{2}(E_x \pm iE_y)}{2}$ refers to the left and right circular polarized light. It indicates that when the linear or left/right circular polarized light is used as the pump beam, only the component of the excitation field that aligns with the polarization state of the pump light is effectively detected. The polarization-aligned nonlinear field component exhibits a much higher intensity than the orthogonal component which can be regarded as background noise.

For $E_{spp,z}$, it can be expressed by $E_{spp,x}$ and $E_{spp,y}$ via the gradient of the components of the vector field derived from the Maxwell equation[28], which can be obtained from our method. Based on the obtained electric field distributions, the spin angular momentum S can be further calculated owing to the inherent relationship between E and H of the SPPs[29].

In this work, the simulation is performed by the commercial softsware FDTD Solutions from Lumerical Solutions Inc. In the simulation, the source power needs to be large enough to generate the third-order nonlinear signal, and therefore the electric field strength is set as 1000 V/m. In addition, to mitigate the impact of the spectral expansion of the light source on the relatively weak nonlinear signals, it is essential to consider the spectral domain of the excitation light during the configuration of the pulse, for which the pulse width is set as 120fs.

As an example, a concentric ring structure fabricated on the gold film is simulated, as shown in Fig. 2(a). In the model, the wavelength of pump light is set as 800 nm, and the excitation light is set as 1030 nm. The thickness of the gold film is set as 150 nm, the slot width of the groove is set as w=508.5 nm(λ_{spp}/2), the grating period is d=1017 nm(λ_{spp}), and the radius of the minimum ring is 8 μm. The depth of the grooves is 150 nm, which means the gold layer is entirely etched. In terms of material model setup, we

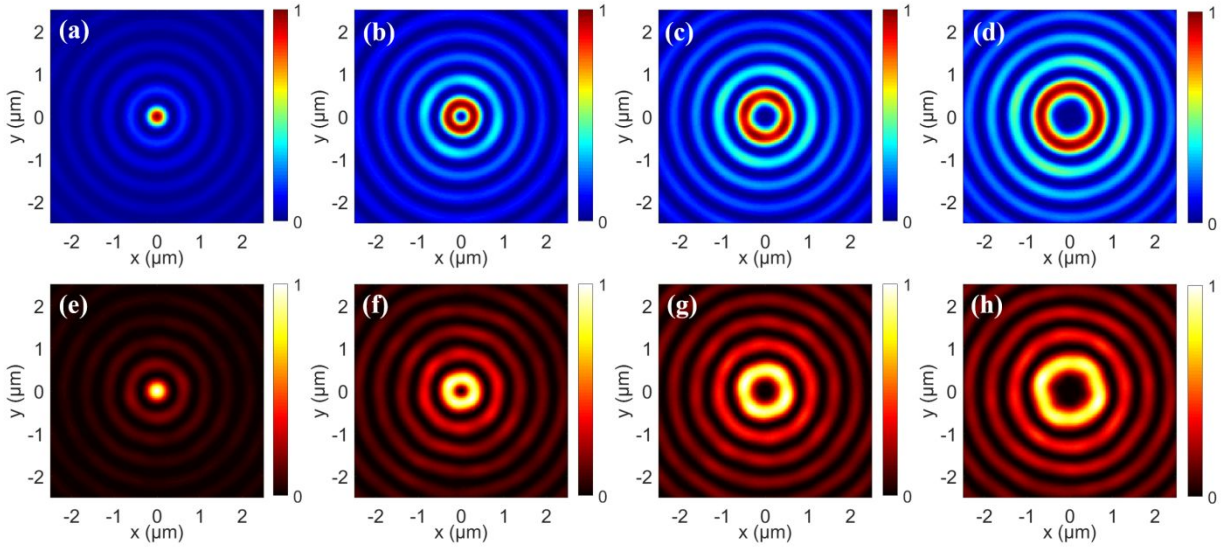

Fig. 3 (a–d) The right circular polarized component of the SPP field generated by the radially polarized light of *l*(*l*=1~4) order vortex incident on the grating. (e–h) The nonlinear signal when the pump light is set as right circular polarized.

chose to use the built-in Chi2/Chi3 model and Au(gold-Johnson and Christy) as the base material.

The SPP field is excited by a radially polarized light with third-order vortex (l=3) and λ=1030 nm. The x-polarized pump light with λ=800 nm is incident vertically into the unstructured area in the center, and the nonlinear signal with λ=654 nm is generated. The calculated results of the extracted nonlinear signal light field are influenced by the nonlinear coefficients. Improper setting of the nonlinear coefficients can lead to errors in the simulation process. When the coefficient is excessively high, the generated nonlinear field acts as a secondary source in the simulation, leading to simulation collapse, as shown in Fig. 2(c). Conversely, if the nonlinear coefficient is too low, the nonlinear signal cannot be detected, as shown in Fig. 2(h). As shown in Fig. 2(d–g), the simulation results of the nonlinear signals obtained from this procedure align well with near-field distribution in Fig. 2(b) over a significant range of the nonlinear coefficients. The appropriate setting of the nonlinear coefficients depends on the system settings in different simulation environments. In the following parts of this work, the second-order nonlinear coefficients are set as 0, and the third-order nonlinear coefficients are set as 10^{-7} $(m/V)^2$. This allows the simulation process to accurately respond to the intensity mapping of the nonlinear field while ensuring the overall convergence and stability of the simulation.

3. Result

Firstly, we utilize the constructed simulation model to calculate the nonlinear signals from the evanescent fields of the cylindrical vector vortex beams. The sample is a concentric ring structure fabricated on the gold film as shown in Fig. 2(a). The radially polarized light carrying optical vortex with different topological orders l is used to illuminate the structure, generating SPP vortex with various light field structures. The excitation light source is sufficiently large to adequately cover the grating structure, enhancing the intensity of the evanescent wave. Since the polarization state of the light varies angularly and a polarization singularity exists at the geometric center of the light source, it is necessary to align the geometric center of the light source with the center of the structure to create an ideal symmetrical vector light field. When the geometric positions of the light source and the grating structure are correctly set, the generated evanescent wave propagates in the direction of the concentric circle radius. The near-field right circular polarized component of the electric field of the SPP vortex with l=1,2,3,4 at the wavelength of λ=1017 nm is shown in Fig. 3(a–d), respectively. It is found that the singularity in the central area increases in size as the topological order l increases. The presence of singularities indicates that the light field carries orbital angular momentum, which can exert rotational torque on particles[30]. Furthermore, the intensity gradient formed in space generates light pressure, allowing tiny particles to be trapped and moved[31]. The size of the pump light source is confined to the flat area of the structure within The concentric circles to prevent direct interaction with the excitation light passing through the groove. When the pump light is set as right circular polarized, the right circular polarized component of the near-field electric field is extracted. The corresponding nonlinear signals at the wavelength of λ=654 nm are shown in Fig. 3(e–h), which are consistent with the near-field results in Fig. 3(a–d). In future experiments, the topological order can be controlled dynamically by the spatial light modulator, and the direct imaging of the near-field SPP vortex through NNOM can facilitate the real-time precise manipulation of nanoparticles in the light field gradient at the subwavelength scale.

Secondly, another type of SPP beam with self-focusing characteristics and particle manipulation capability has also been designed and generated. The PWB is a special type of diffraction-free beam that can maintain its shape, intensity distribution, and focusing effect during propagation. By altering the input conditions, the characteristics such as shape, direction, and degree of focusing can be modulated and enhanced local field strength can be generated at a specific location, which is suitable for optical trapping and imaging. Here, we employ the angular spectrum synthesis method to generate the PWB, as depicted in Fig. 4(a). According to the approach described in Ref. [32], the groove structure is set using the angular spectrum of PWB. The focusing position of the designed beam is at the coordinate origin, which is denoted as O in Fig. 4(a). The groove corresponding to the first-order component of the beam's angular spectrum (the phase π) is located on the x-axis at a distance of 15 μm from the origin, and the distance from the origin varies with the angular spectrum angle. The width of the engraved groove is selected to match the excitation wavelength as w=508.5 nm(λ_{spp}/2). The excitation light source for generating the evanescent field is set as x-polarized light, covering all the grooves to generate SPP waves. The SPP wave generated is focused inward within the arc and the phase

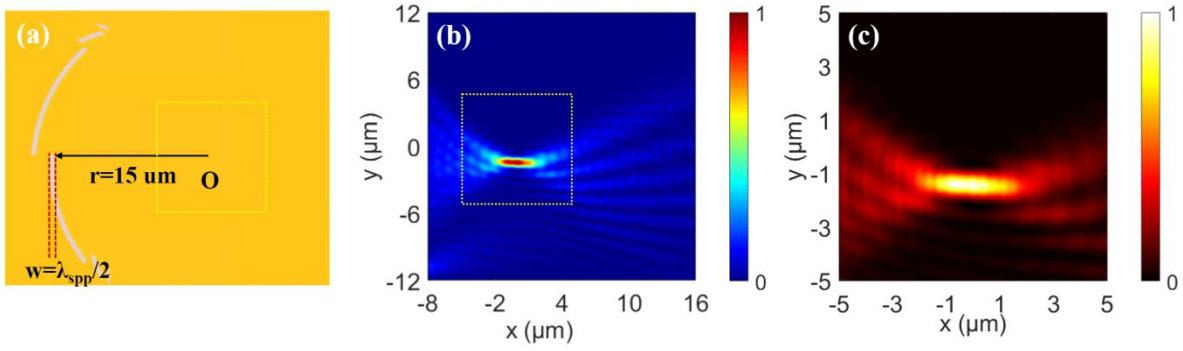

Fig. 4 (a) The structure to generate PWB is designed based on the principle of Fourier Angle spectrum synthesis. O is the origin of the coordinates. (b) PWB excited under X linear polarized light. (c) nonlinear signal (yellow dash area in (a) and (b)) obtained under X linear polarized pump light.

from each part of the arc is precisely controlled by the distance from O. As the phase of the evanescent wave at the focal point varies with the angle, it interferes with the designed angular spectrum component to produce the PWB shown in Fig. 4(b). The x-polarized pump beam is placed at the focusing position of the PWB and away from the grooves (yellow dash area in Fig. 4(a)) to extract the x-polarized component in the PWB. The nonlinear signal obtained from the constructed simulation model is consistent with the marked area in Fig. 4(b), as shown in Fig. 4(c). The generated PWB exhibits a marked local enhancement and

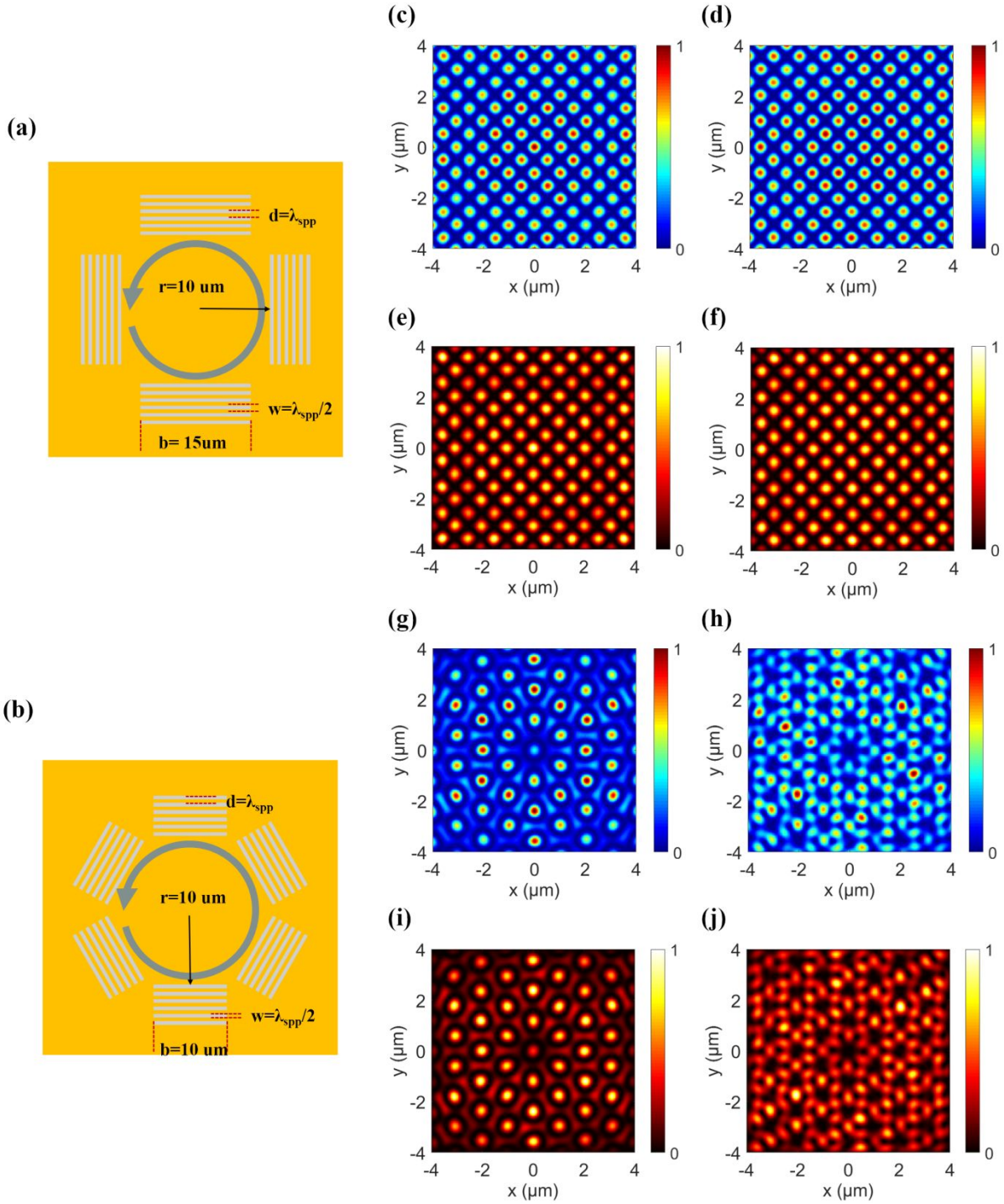

Fig. 5 (a, b) The quadrilateral and hexagonal grating respectively. The blue circular arrow represents the polarization direction of the excitation light, which is left circular polarized. (c, d) Left circular polarized and right circular polarized components of SPP field generated by the quadrilateral grating under left circular polarized excitation light. (e, f) The corresponding nonlinear signal generated under the right and left circular polarized pump light. (g–j) The corresponding results for the hexagonal grating.

non-diffractive characteristic, with the beam shape being maintained in the Y direction. Similarly, the scanning-less detection of the near-field light field of the PWB provides a vital tool for potential applications of PWB including dynamic manipulation of optical trapping at the subwavelength scale.

Moreover, calculation of the spin textures of the photonic spin meron and skyrmion lattices are demonstrated. As depicted in Fig.5 (a) and (b), the quadrilateral and the hexagonal structures consisting of parallel gratings are constructed on the gold film. In each unit of parallel grating, the grating period is set as d=1.017μm (λ_{spp}), the length is 15 μm and 10 μm for quadrilateral and hexagonal structures respectively, the fill factor is 0.5, the number of gratings is 5, and the distance from the nearest grating to the center is 10 μm. The excitation light source is set as left circular polarized, and the SPP excited by the gratings propagates along the direction perpendicular to the gratings and interferes in the flat area at the center. The left and right circular polarized light are utilized as the pump light with the illuminated area of the light source confined within the central flat area, and the corresponding nonlinear signals are demonstrated in Fig. 5 (e,f) and (i,j), respectively, which are consistent with the near-field left and right circular polarized components of the SPP fields as shown in Fig. 5 (c,d) and (g,h The photonic spin topologies are determined by the field symmetries, and therefore through the quadrilateral and hexagonal gratings as shown in Fig. 5 (a) and (b) the photonic spin meron lattice with four-fold symmetry and the photonic spin skyrmion lattice with six-fold symmetry can be generated respectively[33]. For the photonic spin textures, after the left and right circular polarized components of SPP fields are extracted, the longitudinal component of the spin angular momentum can be calculated, and the 3D spin vector distribution can be reconstructed[29]. Recently, the transformation between different topological states of photonic skyrmion has been realized on the same sample[34], but the experiment still relied on the NSOM system and the field polarizations cannot be differentiated. In the future, based on the guidance provided by the simulation tool proposed in this work, the dynamic observation of the spin structures of the different topological states on the same sample can be realized, which not only sheds light on the physical insight of the topological transformation but also contributes to the development of photonic-skyrmion-related applications.

4. Conclusion

In summary, the direct far-field imaging of the near-field distributions of the structured light fields through the nonlinear FWM effect has been investigated in this work. A FDTD simulation model has been constructed through the analysis of the setting of the incident source and the third-order nonlinear coefficients of the FWM process. By modulating the polarization state of the pump light, different near-field in-plane polarization components can be selectively retrieved for a wide range of structured light fields including cylindrical vector vortex beams, PWBs, and topological spin textures. By constructing concentric gratings on gold film, we employed the generated nonlinear signal to illustrate the intensity variations of vortex light fields with different topological charges (l=1~4), exhibiting possibility of dynamic manipulation of nanoparticle in the light field gradient at the subwavelength scale. In addition, we detected PWBs characterized by non-diffractive and self-focusing properties, produced using the angle spectrum synthesis method, demonstrating the potentials for real-time manipulation of the local enhancement point. Moreover, we generated photonic spin meron and skyrmion lattices using four-fold and six-fold symmetric grating structures, respectively. Two orthogonal circular polarization components were extracted from their evanescent fields, which are essential for mapping of the 3D spin vector distribution and investigation of the spin-orbit interaction phenomena in topological spin textures. For the structured light fields simulated above, the nonlinear signals are all consistent with the corresponding near-field polarization components. This work provides guidance for the scanning-less NNOM experiment of various kinds of latest emergent structured light fields, which opens new avenues for deeper insights into the light-matter interaction at nanoscale, as well as advanced applications such as optical tweezers, non-diffractive beams, and optical information processing.

Funding Sources

This work was supported by Guangdong Major Project of Basic Research (2020B0301030009); the National Natural Science Foundation of China (62075139, 61935013, 12004260); Natural Science Foundation of Guangdong (2024A1515012503); Innovation Team Project of Ordinary University of Guangdong Provincial Education Bureau (2024KCXTD014); Science and Technology Innovation Commission of Shenzhen (RCJC20200714114435063); Research Team Cultivation Program of Shenzhen University (2023QNT012); Shenzhen University 2035 Initiative (2023B004).

Reference

1. E. A. Ash and G. Nicholls, "Super-resolution Aperture Scanning Microscope," Nature **237**, 510-512 (1972).
2. K. Kurihara, H. Ohkawa, Y. Iwasaki, O. Niwa, T. Tobita, and K. Suzuki, "Fiber-optic conical microsensors for surface plasmon resonance using chemically etched single-mode fiber," Anal. Chim. Acta **523**, 165-170 (2004).
3. S. Onishi, K. Matsuishi, J. Oi, T. Harada, M. Kusaba, K. Hirosawa, and F. Kannari, "Spatiotemporal control of femtosecond plasmon using plasmon response functions measured by near-field scanning optical microscopy (NSOM)," Opt. Express **21**, 26631-26641 (2013).
4. Y.-C. Yong, Y.-Z. Wang, and J.-J. Zhong, "Nano-spectroscopic imaging of proteins with near-field scanning optical microscopy (NSOM)," Curr. Opin. Biotechnol. **54**, 106-113 (2018).
5. C. Luo, X. Guo, H. Hu, D. Hu, C. Wu, X. Yang, and Q. Dai, "Probing Polaritons in 2D Materials," Adv. Opt. Mater. **8**, 1901416 (2020).
6. D. A. Vanden Bout, J. Kerimo, D. A. Higgins, and P. F. Barbara, "Near-Field Optical Studies of Thin-Film Mesostructured Organic Materials," Acc. Chem. Res. **30**, 204-212 (1997).
7. C. R. McNeill, H. Frohne, J. L. Holdsworth, J. E. Furst, B. V. King, and P. C. Dastoor, "Direct Photocurrent Mapping of Organic Solar Cells Using a Near-Field Scanning Optical Microscope," Nano Lett. **4**, 219-223 (2004).
8. A. J. Das, R. Shivanna, and K. S. Narayan, "Photoconductive NSOM for mapping optoelectronic phases in nanostructures," Nanophotonics **3**, 19-31 (2014).
9. S. Smith, N. C. R. Holme, B. Orr, R. Kopelman, and T. Norris, "Ultrafast measurement in GaAs thin films

using NSOM," Ultramicroscopy **71**, 213-223 (1998).
10. L. Baird, G. H. Ang, C. H. Low, N. M. Haegel, A. A. Talin, Q. Li, and G. T. Wang, "Imaging minority carrier diffusion in GaN nanowires using near field optical microscopy," Physica B **404**, 4933-4936 (2009).
11. P.-K. Wei, Y.-C. Chen, and H.-L. Kuo, "Systematic variation of polymer jacketed fibres and the effects on tip etching dynamics," J. Microsc. **210**, 334-339 (2003).
12. J. Yang, J. Zhang, Z. Li, and Q. GONG, "Fabrication of high-quality SNOM probes by pre-treating the fibres before chemical etching," J. Microsc. **228**, 40-44 (2007).
13. R. Niemann, N. S. Mueller, S. Wasserroth, G. Lu, M. Wolf, J. D. Caldwell, and A. Paarmann, "Spectroscopic and Interferometric Sum-Frequency Imaging of Strongly Coupled Phonon Polaritons in SiC Metasurfaces," Advanced Materials **36**, 2312507 (2024).
14. K. Frischwasser, K. Cohen, S. Tsesses, S. Dolev, G. Rosenblatt, and G. Bartal, "Nonlinear Forced Response of Plasmonic Nanostructures," Physical Review Letters **128**, 103901 (2022).
15. L. Du, A. Yang, A. V. Zayats, and X. Yuan, "Deep-subwavelength features of photonic skyrmions in a confined electromagnetic field with orbital angular momentum," Nat. Phys. **15**, 650-654 (2019).
16. S. Tsesses, E. Ostrovsky, K. Cohen, B. Gjonaj, N. H. Lindner, and G. Bartal, "Optical skyrmion lattice in evanescent electromagnetic fields," Science **361**, 993-996 (2018).
17. Q. Zhang, Z. Xie, P. Shi, H. Yang, H. He, L. Du, and X. Yuan, "Optical topological lattices of Bloch-type skyrmion and meron topologies," Photonics Res. **10**, 947-957 (2022).
18. A. Ghosh, S. Yang, Y. Dai, Z. Zhou, T. Wang, C.-B. Huang, and H. Petek, "A topological lattice of plasmonic merons," Appl. Phys. Rev. **8**, 041413 (2021).
19. Y. Shen, B. Yu, H. Wu, C. Li, Z. Zhu, and A. Zayats, "Topological transformation and free-space transport of photonic hopfions," Adv. Photonics **5**, 015001 (2023).
20. H. Wang and S. Fan, "Photonic Spin Hopfions and Monopole Loops," Phys. Rev. Lett. **131**, 263801 (2023).
21. P. Ornelas, I. Nape, R. de Mello Koch, and A. Forbes, "Non-local skyrmions as topologically resilient quantum entangled states of light," Nat. Photonics **18**, 258-266 (2024).
22. A. Yang, X. Lei, P. Shi, F. Meng, M. Lin, L. Du, and X. Yuan, "Spin-Manipulated Photonic Skyrmion-Pair for Pico-Metric Displacement Sensing," Adv. Sci. **10**, 2205249 (2023).
23. X. Lei, L. Du, X. Yuan, and A. V. Zayats, "Optical spin–orbit coupling in the presence of magnetization: photonic skyrmion interaction with magnetic domains," Nanophotonics **10**, 3667 - 3675 (2021).
24. H. Hu, A. K. Pal, A. Berestennikov, T. Weber, A. Stefancu, E. Cortés, S. A. Maier, and A. Tittl, "Surface-Enhanced Raman Scattering in BIC-Driven Semiconductor Metasurfaces," Adv. Opt. Mater. **12**, 2302812 (2024).
25. K. He, Q. Niu, Y. Xie, S. Xiao, Y. Yang, and J. Zhu, "Bound state in the continuum (BIC) excited by the metasurface breaking in-plane symmetry and quasi-BIC for terahertz sensing," Appl. Phys. Lett. **124**, 231702 (2024).
26. Á. R. Echarri, J. D. Cox, F. Iyikanat, and F. J. G. d. Abajo, "Nonlinear plasmonic response in atomically thin metal films," Nanophotonics **10**, 4149-4159 (2021).
27. K. Frischwasser, K. Cohen, J. Kher-Alden, S. Dolev, S. Tsesses, and G. Bartal, "Real-time sub-wavelength imaging of surface waves with nonlinear near-field optical microscopy," Nat. Photonics **15**, 442-448 (2021).
28. T. J. Davis, D. Janoschka, P. Dreher, B. Frank, F.-J. Meyer zu Heringdorf, and H. Giessen, "Ultrafast vector imaging of plasmonic skyrmion dynamics with deep subwavelength resolution," Science **368**, eaba6415 (2020).
29. C. C. Li, P. Shi, L. P. Du, and X. C. Yuan, "Mapping the near-field spin angular momenta in the structured surface plasmon polariton field," Nanoscale **12**, 13674-13679 (2020).
30. C. Bin, L. Kelbauskas, S. Chan, R. M. Shetty, D. Smith, and D. R. Meldrum, "Rotation of single live mammalian cells using dynamic holographic optical tweezers," Opt. Lasers Eng. **92**, 70-75 (2017).
31. N. B. Vilas, P. Robichaud, C. Hallas, G. K. Li, L. Anderegg, and J. M. Doyle, "An optical tweezer array of ultracold polyatomic molecules," Nature **628**, 282-286 (2024).
32. S. S. Kou, G. Yuan, Q. Wang, L. Du, E. Balaur, D. Zhang, D. Tang, B. Abbey, X.-C. Yuan, and J. Lin, "On-chip photonic Fourier transform with surface plasmon polaritons," Light Sci. Appl. **5**, e16034 (2016).
33. X. Lei, A. Yang, P. Shi, Z. Xie, L. Du, A. V. Zayats, and X. Yuan, "Photonic Spin Lattices: Symmetry Constraints for Skyrmion and Meron Topologies," Phys. Rev. Lett. **127**, 237403 (2021).
34. M. Lin, Q. Liu, H. Duan, L. Du, and X. Yuan, "Wavelength-tuned transformation between photonic skyrmion and meron spin textures," Appl. Phys. Rev. **11**, 021408 (2024).